

HISTORY FORCE AND INERTIA EFFECTS APPLIED TO SWIRLING FLOW PRODUCED WATER TREATMENT

Dirk F. VAN EIJKEREN* and Harry W.M. HOEIJMAKERS†

University of Twente, Faculty of Engineering Technology, Enschede, THE NETHERLANDS

* Corresponding author, E-mail address: d.f.vaneijkeren@utwente.nl

† E-mail address: h.w.m.hoeijmakers@utwente.nl

ABSTRACT

During production of oil, an in time increasing quantity of water is produced. To be able to return produced water to the well or dispose it to the environment, polluting materials have to be separated to the extent that the efflux complies to certain specifications. To be able to remove small quantities of polluting materials, enhanced separation methods are required, such as, flotation, ultra-filtration or swirling flow separation. Produced water can be considered a dilute multiphase fluid. For such fluids it is appropriate to apply Lagrangian particle tracking to predict the trajectories of the dispersed phase, and therewith its distribution.

In Lagrangian particle tracking the force on the particle is approximated by models for effects such as drag, lift and added mass. The history force corrects the drag force for effects of unsteady particle motion. For low Reynolds numbers, the drag can be approximated assuming Stokes' flow about the particle. For higher Reynolds numbers, this assumption is not valid, and it is obtained instead from semi-empirical correlations. Present research investigates differences in predicted trajectories and separation efficiency that can be observed taking into account non-Stokesian effects for the drag as well as history effects for typical oil-droplets in a typical flow field observed during swirling flow separation processes.

Keywords: Dispersed droplet dynamics, separation, Lagrangian particle tracking, history force, drag coefficient .

NOMENCLATURE

a	Particle acceleration	$[m\ s^{-2}]$
D	Particle diameter	$[m]$
f	Drag factor	$[-]$
f	Volumetric force per unit mass	$[m\ s^{-2}]$
F	Force	$[N]$
h	History acceleration	$[m\ s^{-2}]$
K	Dimensionless kernel for history integral	$[-]$
m	Particle mass	$[kg]$
R	Pipe radius	$[m]$
Re	Diameter based particle Reynolds number	$[-]$
s	Integration time	$[s]$
t	Time	$[s]$
T	Dimensionless history time	$[-]$
u	Flow field velocity	$[m\ s^{-1}]$
v	Particle velocity	$[m\ s^{-1}]$
w	Relative velocity $\mathbf{v} - \mathbf{u}$	$[m\ s^{-1}]$
U	Reference velocity	$[m\ s^{-1}]$

x	Location of the particle centre of mass	$[m]$
Γ	Circulation	$[m^2\ s^{-1}]$
ρ	Mass density	$[kg\ m^{-3}]$
σ	Stress tensor	$[Pa]$
ν	Kinematic viscosity	$[m^2\ s^{-1}]$
τ	Characteristic time, integration time	$[s]$

INTRODUCTION

In the oil industry, water is used to maintain the pressure in oil reservoirs during the extraction of oil. Therefore, an in time increasing quantity of water is produced. Separation of this oil-water mixture is required to recover the desired oil. Moreover, to be able to return produced water to the well or dispose it to the environment, polluting materials have to be separated up to certain specifications. Separation of phases is achieved in several stages. The first stage is bulk separation, in which the mixture is separated in the two phases with a residual of the other phase remaining. Secondary separation is then required for the removal from the oil or water bulk of the undesired pollution of water-in-oil or oil-in-water, respectively. To be able to remove small quantities of polluting materials, enhanced separation methods are required, such as, flotation, ultra-filtration and swirling flow separation. During produced water treatment the oil-water mixture can be considered a dilute multiphase fluid. For such fluids it is appropriate to apply Lagrangian particle tracking to predict the oil-droplet trajectories that determine the distribution of the dispersed phase.

Conventional methods, such as gravity settlers, used to achieve phase separation are not adequate for produced water treatment for which droplets are quite small. Therefore, advanced methods have been developed, such as swirling flow separators and flotation tanks. In swirling flow separators, the driving force is the hydrodynamic stress-gradient. This results in reduced settling times at the cost of a complex flow field. Flotation tanks, in which oil droplets adhere to rising gas bubbles utilize the effective density of the oil-gas dispersed phase to decrease settling time. However, chemical phenomena can have a significant impact on flotation performance.

To control the efficiency of separators, it is not only necessary to be able to accurately predict the flow field of the continuous phase in the separator, but also to be able to accurately predict the droplet trajectories. Small changes in particle trajectories could imply having to adjust design requirements for the separator device, such as shape and size.

Therefore, in the present study the forces in the equations of motion for a particle have been investigated in order to enable the prediction of particle behaviour adequately. Present study involves particle behaviour in a flow field typical for swirling flow separators. Effects of emulsions and surfactants can be included by adapting the correlations.

In the present research the force on the oil droplets in water is approximated assuming the oil-droplets to behave as spherical solid particles. For these particles the drag force and the history force, which arise in Lagrangian particle tracking, have been investigated. Particle trajectories have been predicted using various drag coefficient correlations, with and without taking the history force into account. Moreover, the history force has been predicted with and without the assumption of Stokes' flow. The parameters contained in the expression for the history force are investigated using experimental data found in literature, e.g. (Mordant and Pinton, 2000). Effects of lift might be important, but are not yet considered in the present study.

MODEL DESCRIPTION

Forces exerted by the fluid on the particle result in acceleration of the particle, while the motion of the particle influences the motion of the fluid as well. However, the fluid motion on a scale much larger than the particle is barely influenced by the presence and motion of the particle. Therefore, it is assumed that we may use one-way coupling, i.e. the fluid motion drives particle motion but not vice versa. First, an analytic description will be provided for the averaged large scale fluid motion typically observed in swirling flow separators. Subsequently the equations of motion for the particle will be derived. Finally the numerical procedure to obtain the solution of the equations of motion as well as the history force integral are provided.

Swirling flow field

A flow field typically observed in a swirling flow separator consists of a combination of the velocity due to a solid body rotation and that of an inviscid vortex, a so-called Lamb-Oseen vortex. Moreover, observed axial flow fields typically consist of a W-shaped profile (Slot *et al.*, 2012). In the present research the flow field mimics an in-line swirling flow separator with constant radius, with axial and azimuthal velocity distributions that remain the same in axial direction. As a result, the radial velocity will be zero.

A Lamb-Oseen vortex for a fluid with kinematic viscosity ν results in the required azimuthal velocity field with circulation Γ and viscous decay-time τ_v . The W-shaped axial velocity profile with maximum velocity U , a reverse flow velocity parameter U_0 and a parameter U_1 that gives the central jet velocity as well as a second viscous decay-time in the core $\tau_{v,1}$ results in the required axial flow field. Therefore, the fluid velocity becomes

$$\begin{pmatrix} u_r \\ u_\theta \\ u_z \end{pmatrix} = \begin{pmatrix} 0 \\ \frac{\Gamma}{2\pi r} \left(1 - e^{-\frac{r^2}{\tau_v \nu}}\right) \\ U - U_0 e^{-\frac{r^2}{\tau_v \nu}} + U_1 e^{-\frac{r^2}{\tau_{v,1} \nu}} \end{pmatrix}. \quad (1)$$

The velocity in axial direction should result in a volume flow equal to the volume flow in a pipe with radius R and

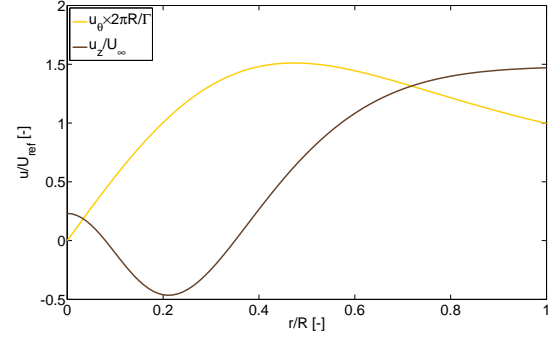


Figure 1: The tangential and axial velocity in equation (1) using parameters as in table 1.

τ_v [s]	Γ [m^2s^{-1}]	ν [m^2s^{-1}]	R [m]
500	2	8.92×10^{-7}	0.05
$\tau_{v,1}$ [s]	U_∞ [m s^{-1}]	U_0 [m s^{-1}]	U_1 [m s^{-1}]
$\frac{250}{3}$	2	6	$\frac{7}{2}$

Table 1: Parameters used for swirling flow.

bulk velocity U_∞ . This implies that for chosen U_0 and U_1 , the maximum velocity becomes

$$U = U_\infty + U_0 \frac{\tau_v \nu}{R^2} \left(1 - e^{-\frac{R^2}{\tau_v \nu}}\right) - U_1 \frac{\tau_{v,1} \nu}{R^2} \left(1 - e^{-\frac{R^2}{\tau_{v,1} \nu}}\right). \quad (2)$$

The parameters, selected to mimic typical flow conditions in a swirling flow separator, including features such as flow reversal, are shown in table 1. The resulting velocity profiles are shown in figure 1.

Equation of motion for particle

The motion of a particle is governed by the forces acting on the particle. Newton's second law applied to the motion of the particle states that

$$\frac{d}{dt} (m\mathbf{v}) = \mathbf{F}_{\text{particle}}, \quad (3)$$

with \mathbf{v} the particle velocity, and m the mass of the particle subjected to force $\mathbf{F}_{\text{particle}}$. As the lift forces are not considered in the present research, the equation of motion for the rotation of the particle will not be considered either.

Volumetric forces and the surface stresses of the fluid contribute to the force on the particle. The volumetric force per unit mass \mathbf{f} is usually the gravitational acceleration \mathbf{g} . The stress $\boldsymbol{\sigma}$ at the surface of the particle results from the motion of the fluid about the particle, consisting of the pressure and the viscous stress. This implies that the surface stress can only be obtained if the motion of the fluid about the particle is fully resolved. For most practical applications this is not feasible. Therefore, the surface integral is approximated by a sum of forces, each representing separate effects of the flow field as well as of the particle motion. These forces depend on the large-scale flow field in the

absence of particles, represented by the flow variables and their derivatives at the location, \mathbf{x} , of the centre of mass of the particle. The effects taken into account in the present research are the volumetric forces, drag, stress gradient, added mass and the history force. Therefore the force on the particle is approximated by

$$\mathbf{F}_{\text{particle}} \approx \mathbf{F}_{\text{volume}} + \mathbf{F}_{\nabla\sigma} + \mathbf{F}_{\text{AM}} + \mathbf{F}_{\text{D}} + \mathbf{F}_{\text{H}}. \quad (4)$$

The volumetric force is the approximation of a volume integral of volumetric forces such as gravity, while the sum of the other forces is the approximation of the surface integral of the surface stress.

Volumetric, stress gradient and added mass force

The volumetric force contribution is

$$\mathbf{F}_{\text{volume}} = m\mathbf{f}. \quad (5)$$

The stress gradient force $\mathbf{F}_{\nabla\sigma}$, called the pressure gradient force in absence of viscous stresses, represents the surface integral of the stress of the large scale flow field acting at the surface of the particle, i.e. the surface integral of $\sigma \cdot \mathbf{n}$. Using the divergence theorem, the surface integral of the normal component of a vector quantity can be expressed as a volume integral over the volume enclosed by that surface. Therefore, the surface integral of the normal component of the stress acting at the surface can be expressed as the volume integral of the divergence of the stress. For a fluid with velocity \mathbf{u} the stress divergence is subsequently rewritten in terms of the material derivative of the velocity $\frac{D\mathbf{u}}{Dt}$ and the volumetric force \mathbf{f} using the Navier-Stokes equations. With $\frac{m}{\rho_{\text{particle}}}$ as the volume of the particle, this results in

$$\mathbf{F}_{\nabla\sigma} = \frac{m}{\rho_{\text{particle}}} \nabla \cdot \sigma = \frac{m}{\hat{\rho}} \left\{ \frac{D\mathbf{u}}{Dt} - \mathbf{f} \right\}, \quad (6)$$

with the material derivative defined as

$$\frac{D}{Dt} \equiv \frac{\partial}{\partial t} + \mathbf{u} \cdot \nabla, \quad (7)$$

and the density ratio $\hat{\rho}$ defined as

$$\hat{\rho} \equiv \frac{\rho_{\text{particle}}}{\rho_{\text{continuous}}}. \quad (8)$$

The volumetric force (5) and the stress gradient (6) are often combined, leading to the sum of what is often called the buoyancy force and a hydrodynamic stress gradient force

$$\mathbf{F}_{\text{Buoyancy}} + \mathbf{F}_{\nabla\sigma, \text{dynamic}} = \frac{m}{\hat{\rho}} \left\{ (\hat{\rho} - 1)\mathbf{f} + \frac{D\mathbf{u}}{Dt} \right\}. \quad (9)$$

A difference in acceleration of the particle relative to the large scale fluid motion, results in about an equal volume of the continuous phase to be accelerated in the direction opposite to that of the relative acceleration. This causes the particle to react as if it is heavier than its actual mass. Therefore this force is called, the added, or virtual mass effect,

$$\mathbf{F}_{\text{AM}} = C_{\text{AM}} \frac{m}{\hat{\rho}} \left(\frac{D\mathbf{u}}{Dt} - \frac{d\mathbf{v}}{dt} \right). \quad (10)$$

The added mass coefficient for a spherical particle equals $C_{\text{AM}} = \frac{1}{2}$ for the inviscid flow limit, (Auton *et al.*, 1988). This added mass coefficient has been shown to be accurate for a wide range of Reynolds numbers, (Loth and Dorgan, 2009).

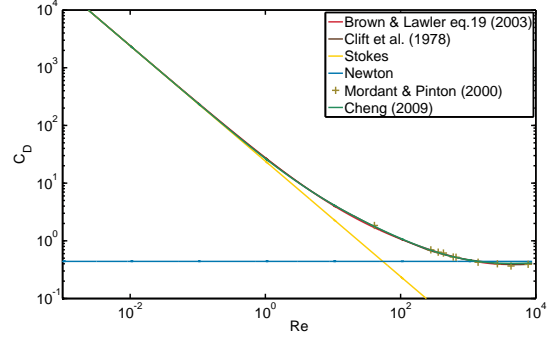


Figure 2: Drag coefficients as a function of Re . Experimental data by (Mordant and Pinton, 2000).

Drag force

The drag approximates the effect that the particle tends to follow the motion of the fluid. Both viscous drag due to boundary layer development as well as pressure drag due to flow separation at the surface of the sphere are included. Drag expressions commonly involve a drag coefficient C_{D} leading to

$$\mathbf{F}_{\text{D}} = -\frac{m}{\hat{\rho}} \frac{3}{4} \frac{C_{\text{D}}(Re)}{D} |\mathbf{w}| \mathbf{w}, \quad (11)$$

with relative velocity $\mathbf{w} \equiv \mathbf{v} - \mathbf{u}$, and the diameter based particle Reynolds number defined as

$$Re \equiv \frac{D|\mathbf{w}|}{\nu}, \quad (12)$$

with particle diameter D and kinematic viscosity of the continuous phase ν .

The drag force corresponding to Stokes' flow is

$$C_{\text{D}, \text{Stokes}} = \frac{24}{Re}. \quad (13)$$

Drag coefficients that differ from that for Stokes drag can be written as a factor times the Stokes drag coefficient. This is the drag factor, leading to

$$f \equiv \frac{Re}{24} C_{\text{D}}. \quad (14)$$

Therefore, the drag can also be expressed using the drag factor as

$$\mathbf{F}_{\text{D}} = -18 \frac{m}{\hat{\rho}} \frac{f(Re)}{\tau_{\text{d}}} \mathbf{w}, \quad (15)$$

with a diffusive time-scale defined as

$$\tau_{\text{d}} \equiv \frac{D^2}{\nu}. \quad (16)$$

In present research one drag correlation has been used as representing a multitude of drag correlations similar in magnitude over the entire Reynolds number range up to the Reynolds number at which the flow changes to fully turbulent flow at $Re \sim 2 \times 10^5$. This drag factor, by (Cheng, 2009) is

$$f = (1 + 0.27Re)^{0.43} + 0.47 \frac{Re}{24} \left[1 - e^{-0.04Re^{0.38}} \right]. \quad (17)$$

Cheng obtained this drag correlation by a fit of a collection of drag data. This data is the basis for many existing correlations, but note that for this correlation the data has first been corrected for wall effects. It should have higher accuracy than other similar expressions such as (Brown and Lawler, 2003). Moreover, the expression has favourable properties for numerical implementation such as no discontinuities and no singularities for both the drag factor and its derivative. Figure 2 shows several drag coefficients similar to that of Cheng as well as the Stokes drag coefficient and the drag coefficient predicted for the Newton regime. It can be observed that the various drag correlations do not differ much along the shown range of Reynolds numbers. However, Stokes drag clearly starts to deviate more and more for Reynolds numbers larger than about 0.5.

History force

The drag force only depends on the present value of the Reynolds number. Thereby, it assumes fully developed boundary layers and wake. The history force accounts for the lagging transient boundary layer development, as well as that of the particle wake. To capture these transient effects, an integral over time is required from the start of particle motion up to present time. A kernel $K(t, \tau)$ relates the acceleration of the particle at time τ to the resulting force at time t . The force is written as

$$\mathbf{F}_H = -\frac{18m}{\tau_d \hat{\rho}} \int_{-\infty}^t K(t, \tau) \frac{d\mathbf{w}}{d\tau} d\tau. \quad (18)$$

Assuming Stokes' flow, this results in the Basset kernel, e.g. (Crowe *et al.*, 1998),

$$K_{\text{Basset}}(t, \tau) = \frac{1}{\sqrt{4\pi}} \frac{1}{\sqrt{T_{\text{Basset}}(t, \tau)}}, \quad (19)$$

where the Basset history time is defined as

$$T_{\text{Basset}}(t, \tau) \equiv \frac{t - \tau}{\tau_d}. \quad (20)$$

The history force, obtained using this kernel is often called the Basset force. Therefore, the history force obtained with this kernel will subsequently be called the Basset force to distinguish it from a more general history force. The diffusive time scale τ_d is the only fluid flow property that influences the rate of decay of the kernel in time. However, it has been observed that the long time behaviour of the kernel shows a faster decay than the Basset kernel predicts, e.g. (Mei *et al.*, 1991; Loth and Dorgan, 2009; Mordant and Pinton, 2000). As a consequence, the Basset kernel leads to a significant over-prediction of the history force. Therefore, a kernel was proposed, (Mei *et al.*, 1991; Mei and Adrian, 1992), that takes into account effects due to inertia. The kernel was subsequently refined using the drag factor, (Lawrence and Mei, 1995), leading to

$$K_{L\&M}(t, \tau) = \frac{3 [f(t) + \text{Re}(t) f'(t)] f'(\tau)}{\left[\frac{1}{\tau_d} \int_{\tau}^t \text{Re}(s) ds \right]^2}, \quad (21)$$

where

$$f'(t) \equiv \left. \frac{df}{d\text{Re}} \right|_{\text{Re}(t)}. \quad (22)$$

This kernel was adapted to obtain the Basset kernel in the limit of Stokes flow, (van Eijkeren and Hoeijmakers, 2010)

$$K(t, \tau) = \frac{4}{\pi} \frac{f_H(t, \tau)}{\left[\left[\frac{f^2(t) T_H(t, \tau)}{\text{Re}(t)} \right]^{\frac{1}{4}} + T_H(t, \tau) \right]^2}, \quad (23)$$

with the history drag factor defined as

$$f_H(t, \tau) \equiv \frac{3}{4} \pi [f(t) + \text{Re}(t) f'(t)] f'(\tau), \quad (24)$$

and the dimensionless history time

$$T_H(t, \tau) \equiv \frac{1}{\tau_d} \int_{\tau}^t \frac{\text{Re}(s)}{f(s)} ds. \quad (25)$$

Numerical solution method

Equation of motion

The equation of motion to be solved is

$$\begin{aligned} (\hat{\rho} + C_{AM}) \frac{d\mathbf{v}}{dt} &= (\hat{\rho} + C_{AM}) \mathbf{a} \equiv (1 + C_{AM}) \frac{D\mathbf{u}}{Dt} \\ &+ (\hat{\rho} - 1) \mathbf{f} - 18 \frac{f}{\tau_d} \mathbf{w} - \frac{18}{\tau_d} \int_{-\infty}^t K(t, \tau) \frac{d\mathbf{w}}{d\tau} d\tau. \end{aligned} \quad (26)$$

This ODE is discretized using a (Crank and Nicolson, 1996) method. The general formulation for the position and velocity of the particle at time t_{n+1} predicted using time t_n and with $\left. \frac{d\mathbf{v}}{dt} \right|_t \equiv \mathbf{a}(\mathbf{v}, \mathbf{x}, t)$, becomes

$$\begin{pmatrix} \mathbf{x}_{n+1} \\ \mathbf{v}_{n+1} \end{pmatrix} - \begin{pmatrix} \mathbf{x}_n \\ \mathbf{v}_n \end{pmatrix} = \frac{t_{n+1} - t_n}{2} \begin{pmatrix} \mathbf{v}_n + \mathbf{v}_{n+1} \\ \mathbf{a}_n + \mathbf{a}_{n+1} \end{pmatrix}. \quad (27)$$

The system of algebraic equations resulting from this implicit scheme is non-linear, and require iterative solution methods. Solution methods such as Newton, Gauß-Seidel or Jacobi are equal in performance for obtaining a solution.

History integral

The properties of the history integral are a challenge for numerical integration. First, the kernel depends on the upper bound t of the integral. As a consequence the integral evaluated at an earlier time-step cannot be reused for the new time-step. Second, the kernel is singular at the upper bound of the integral, negating the use of standard integration schemes. Also, the lower bound is minus infinity, while information is known only from some time t_0 . Finally, for the non-Stokesian effects, the kernel increases the complexity of the integral.

The problem with the lower bound of minus infinity can be eliminated using partial integration. This results in

$$\int_{-\infty}^{t_0} K(t, \tau) \frac{d\mathbf{w}}{d\tau} d\tau = K_0 \mathbf{w}_0 - \int_{-\infty}^{t_0} \frac{dK(t, \tau)}{d\tau} \mathbf{w} d\tau. \quad (28)$$

Assuming $|\mathbf{w}| = 0$ for $\tau < t_0$ results in an exact expression in which the integral at the right-hand side reduces to zero. Otherwise the integral can only be approximated by zero, and the error depends on time t as well as on the magnitude of the velocity.

ρ_{particle} [kg m ⁻³]	D [m]	$\rho_{\text{continuous}}$ [kg m ⁻³]	g [ms ⁻²]
800	100×10^{-6}	997	0

Table 2: Parameters in performed simulations, continuous flow field as in table 1.

The general integral to be evaluated is of the form $\int_{t_0}^{t_n} \frac{\mathbf{h}}{\sqrt{T}} d\tau$, with $\mathbf{h} \equiv \sqrt{TK} \frac{d\mathbf{w}}{d\tau}$, and T from either equation (20) or (25) for Basset or history force, respectively. A change of variables results in

$$\int_{t_0}^{t_n} \frac{\mathbf{h}}{\sqrt{T}} d\tau = \int_{T_0}^{T_n} \left(\frac{dT}{d\tau} \right)^{-1} \frac{\mathbf{h}}{\sqrt{T}} dT. \quad (29)$$

Partial integration results in

$$\begin{aligned} \int_{T_0}^{T_n} \left(\frac{dT}{d\tau} \right)^{-1} \frac{\mathbf{h}}{\sqrt{T}} dT &= 2\sqrt{T} \left(\frac{dT}{d\tau} \right)^{-1} \mathbf{h} \Big|_{T_0}^{T_n} \\ &\quad - 2 \int_{T_0}^{T_n} \sqrt{T} \frac{d}{dT} \left(\left(\frac{dT}{d\tau} \right)^{-1} \mathbf{h} \right) dT, \end{aligned} \quad (30)$$

where $T_n = 0$ by definition of T . If the derivative in the remaining integral is considered piecewise constant, the discretized integral is obtained

$$\begin{aligned} \int_{t_0}^{t_n} \frac{\mathbf{h}}{\sqrt{T}} d\tau &\approx -2\sqrt{T_0} \left(\frac{dT}{d\tau} \right)_0^{-1} \mathbf{h}_0 \\ &\quad + \frac{4}{3} \sum_{i=0}^{n-1} \left\{ (T_i \sqrt{T_i} - T_{i+1} \sqrt{T_{i+1}}) \right. \\ &\quad \left. \times \frac{\left(\frac{dT}{d\tau} \right)_{i+1}^{-1} \mathbf{h}_{i+1} - \left(\frac{dT}{d\tau} \right)_i^{-1} \mathbf{h}_i}{T_{i+1} - T_i} \right\}. \end{aligned} \quad (31)$$

This discretization can be applied to both the Basset kernel and the full history kernel. Moreover, when a fixed time-step is employed, a discrete Basset kernel can be calculated upfront and only the element for t_0 has to be updated during calculation.

RESULTS

To investigate the influence of non-Stokesian effects as well as the history force, simulations have been performed for an oil-droplet in a swirling flow field with the parameters given in table 1. The properties of the droplet, as well as properties of the continuous phase are specified in table 2.

The resulting particle trajectories in the (r, z) -plane are shown in figure 3. Also, one of the trajectories is shown in the (x, y) -plane in figure 4. Clearly the particle trajectories follow the swirling motion of the flow, while the stress gradient forces the particle towards the axis of rotation. Moreover, when the particle moves towards the axis of rotation, the annular region of reversed flow is reached where the particle is moving in negative z -direction. For even smaller

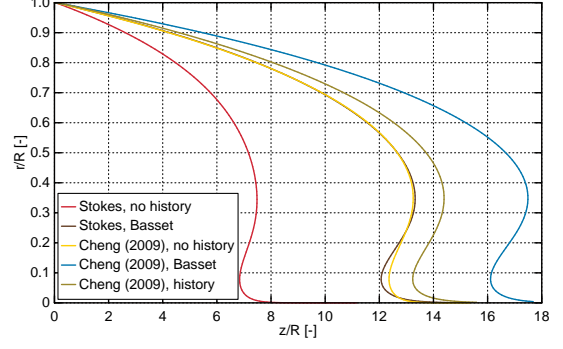


Figure 3: Radial position as a function of the axial position during motion of the particle.

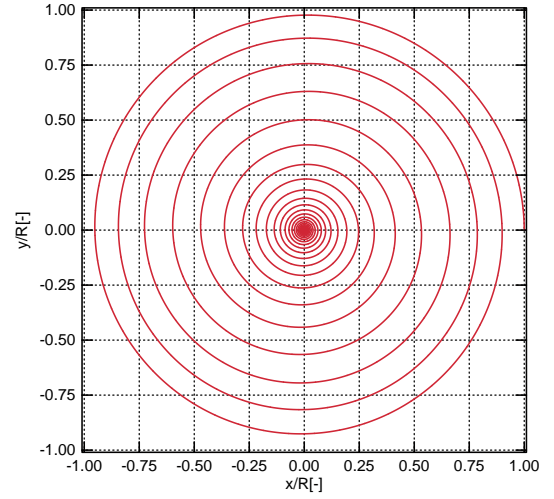


Figure 4: Particle location in the (x, y) -plane during the motion of the particle. Stokes drag without history force.

radii, in the region near the axis of rotation, the particle moves in positive z -direction again.

In figure 3 it is shown that the results of a simulation using Stokes drag do not agree with those of a simulation including non-Stokesian effects. Comparing the results of the simulations, it becomes for example clear that a separator device designed using a more accurate flow simulation, in which non-Stokesian effects have been included in the drag, would have been about a factor 1.8 longer than follows from the flow simulation with just Stokes drag. Including the Basset force for Stokes drag in the calculation of the trajectory, results in a particle trajectory that is remarkably close to the trajectory predicted using the drag coefficient by Cheng. These results indicate that, for the current application, the Basset history force integral might be approximated by a drag-like algebraic expression, which would save computing time.

Furthermore, it can be observed that a droplet trajectory computed using the drag correlation by Cheng, as well as including the Basset force, requires a significantly longer distance in z -direction before the droplet reaches the axis of rotation. However, the Basset force significantly overpredicts the history force. This is concluded from the par-

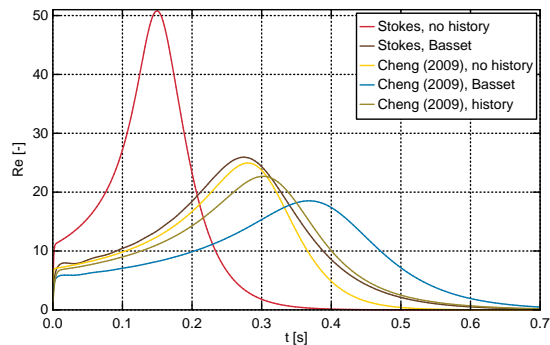


Figure 5: Particle Reynolds number as function of time.

particle trajectory computed including the history force. The extent in z -direction of the particle trajectory is still significantly larger, as is seen when comparing the result to the particle trajectory without including the history force.

Figure 5 presents the Reynolds number for the particle as function of time. The profiles show similar differences as the particle trajectories in the (r, z) plane. For all particle trajectories, the maximum Reynolds number is clearly outside the range in which Stokes drag is assumed to be still accurate. The peak in the Reynolds number becomes lower due to higher values of the drag and history forces. Moreover, with increasing drag, the peak shifts to a later time. This shift is caused by the particle reaching the region of lower stress gradient force later in time.

CONCLUSIONS

In the present paper, Lagrangian simulations have been performed for typical oil-droplets moving in a flow field typical for swirling flow separators. The flow field consists of the azimuthal velocity of a Lamb-Oseen vortex as well as an axial velocity profile with flow reversal. The results obtained employing Stokes drag have been compared with results using an expression for the drag by Cheng, which includes non-Stokesian effects. Furthermore, effects of the history force have been investigated using the Basset kernel, as well as a more general history kernel.

Numerical treatment of the history force with a general history kernel has been described. The numerical treatment deals with the singular behaviour of the integral kernel, as well as with a change to a history time variable. Moreover, dealing with an initial velocity at the start of the calculation is explained in terms of integration by parts.

The results show that Stokes drag is not adequate to obtain accurate particle trajectories for application to swirling flow separation. Moreover, the history force has a significant influence on particle trajectories. These results imply that non-Stokesian effects as well as history effects should be included when predicting particle trajectories in a swirling flow separator. Results also indicate that a drag-like algebraic expression might be sufficient to approximate the history integral in the present type of applications, reducing the computational cost significantly.

ACKNOWLEDGEMENTS

This work was performed by the FACE center, a research cooperation between IFE, NTNU, and SINTEF. The center is funded by The Research Council of Norway, and by the following industrial partners: Statoil, Scandpower Petroleum Technology AS, FMC, CD-Adapco, and Shell Technology Norway AS. The research has been performed at the University of Twente.

REFERENCES

- AUTON, T.R. *et al.* (1988). “The force exerted on a body in inviscid unsteady non-uniform rotational flow”. *Journal of Fluid Mechanics*, **197**, 241–257.
- BROWN, P.P. and LAWLER, D.F. (2003). “Sphere drag and settling velocity revisited”. *Journal of Environmental Engineering*, **129**(3), 222–231. <http://link.aip.org/link/?QEE/129/222/1>.
- CHENG, N.S. (2009). “Comparison of formulas for drag coefficient and settling velocity of spherical particles”. *Powder Technology*, **189**(3), 395–398. <http://www.sciencedirect.com/science/article/pii/S0032591008003719>.
- CRANK, J. and NICOLSON, P. (1996). “A practical method for numerical evaluation of solutions of partial differential equations of the heat-conduction type”. *Advances in Computational Mathematics*, **6**, 207–226. <http://dx.doi.org/10.1007/BF02127704>.
- CROWE, C.T. *et al.* (1998). *Multiphase flows with droplets and particles*. CRC Press, 6000 Broken Sound Parkway, NW, (Suite 300) Boca Raton, Florida 33487, USA. www.crcpress.com.
- LAWRENCE, C.J. and MEI, R. (1995). “Long-time behaviour of the drag on a body in impulsive motion”. *Journal of Fluid Mechanics*, **283**, 307–327. http://journals.cambridge.org/article_S0022112095002333.
- LOTH, E. and DORGAN, A.J. (2009). “An equation of motion for particles of finite Reynolds number and size”. *Environmental Fluid Mechanics*, **9**(2), 187–206.
- MEI, R. and ADRIAN, R.J. (1992). “Flow past a sphere with an oscillation in the free-stream velocity and unsteady drag at finite Reynolds number”. *Journal of Fluid Mechanics*, **237**, 323–341.
- MEI, R. *et al.* (1991). “Unsteady drag on a sphere at finite Reynolds-number with small fluctuations in the free-stream velocity”. *Journal of Fluid Mechanics*, **233**, 613–631.
- MORDANT, N. and PINTON, J.F. (2000). “Velocity measurement of a settling sphere”. *European Physical Journal B*, **18**(2), 343–352.
- SLOT, J.J. *et al.* (2012). “Inline oil-water separation in swirling flow”. *Proceedings of the 8th international conference on CFD in the oil & gas, metallurgical and process industries, Trondheim, 2011*, 121:1–10.
- VAN EIJKEREN, D.F. and HOEIJMAKERS, H.W.M. (2010). “Influence of the history term in a Lagrangian method for oil-water separation”. *7th International Conference on Multiphase Flow - ICMF 2010 Proceedings*, 6.2.1. <http://ufdc.ufl.edu/UF00102023/00147>.